Three-dimensional surface contouring of macroscopic objects by means of phase-difference images

Daniel Velásquez Prieto and Jorge Garcia-Sucerquia

We report a technique to determine the 3D contour of objects with dimensions of at least 4 orders of magnitude larger than the illumination optical wavelength. Our proposal is based on the numerical reconstruction of the optical wave field of digitally recorded holograms. The required modulo 2π phase map in any contouring process is obtained by means of the direct subtraction of two phase-contrast images under different illumination angles to create a phase-difference image of a still object. Obtaining the phase-difference images is only possible by using the capability of numerical reconstruction of the complex optical field provided by digital holography. This unique characteristic leads us to a robust, reliable, and fast procedure that requires only two images. A theoretical analysis of the contouring system is shown, with verification by means of numerical and experimental results.

OCIS codes: 090.0090, 100.5070, 120.4290, 120.6650.

1. Introduction

The noncontact techniques to determine the shape and dimensions of objects under study are a hot topic in optical metrology because of their multiple applications in engineering and science.[1] These methods have been labeled as optical contouring and can be carried out with incoherent illumination (fringe projection,[2] moiré[3,4] or coherent illumination (multiple wavelength,[5] multiple refractive index,[6] or speckle,[7–10] among others).

In the coherent methods, the object's contour is coded in the intensity distribution resulting from an interferometric essay. The interferogram's appearance is determined by characteristics of the interfering waves, and they are managed in such a way that their phase difference provides the information about the contour of the object under study; the effectiveness of the contouring approach relies on the accurate extrapolation of the phase difference from the recorded interferogram. Several methods can be found in the literature to determine the phase difference of interfering waves.[10] The most accurate ones are the numerous versions of phase shifting. All these are based on the numerical computation of the phase difference through the solution of a system of equations with three unknown variables; hence at least three different interferograms with a phase shift between them are required.

In today's optical research and technology, digital holography plays an important role as a tool to numerically compute optical wavefronts from digitally recorded holograms.[11–13] While applications to 3D contouring have been reported by using different approaches such as multiple wavelengths,[14,15] phase shifting,[16,17] tilted illumination,[18] and virtual reference wavefronts,[19] this last approach is possible only by using the numerical capabilities of digital holography.

Since in digital holography the object optical field is calculated as a set of complex numbers, it is possible to obtain amplitude- and phase-contrast images from the recorded holograms. There is great interest in the latter type of image, because with phase-contrast images, the 3D contour of microscopic objects can be determined with nanometric resolutions,[20,21] and absolute refractive indices of microscopic objects (crystals in suspensions) can be evaluated.[22] In the microscopic domain, phase-contrast images can be used quite extensively; however, with large objects, their usefulness is very limited. By large objects, we refer to ones with dimensions of at least 4 orders of magnitude greater

D. Velásquez Prieto is with the Department of Basic Sciences, Universidad EAFIT A.A. 3300, Medellin, Colombia. J. Garcia-Sucerquia (jigarcia@unalmed.edu.co) is with the School of Physics, Universidad Nacional de Colombia Sede Medellin, A.A. 3300, Medellin, Colombia and the Department of Physics, Dalhousie University, Halifax, Nova Scotia B3H 3J5, Canada.

Received 12 December 2005; accepted 16 April 2006; posted 24 April 2006 (Doc. ID 66574).

0003-6935/06/256381-07$15.00/0

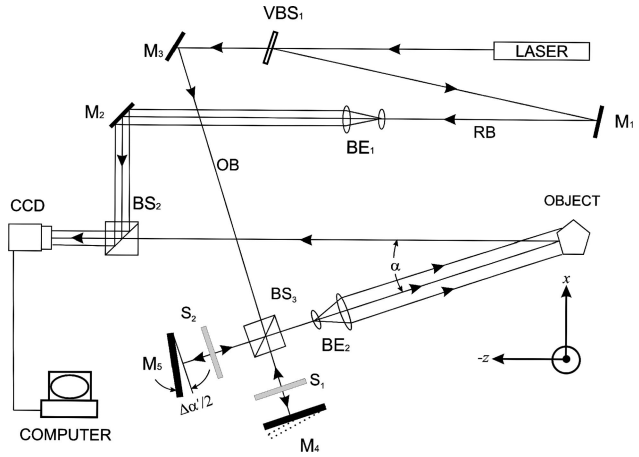

Fig. 1. Schematic representation of the experimental setup; see text for details.

than the wavelength of the optical field. For these objects, direct phase-contrast images take values randomly distributed between $-\pi$ and $+\pi$, since the objects' roughness is comparable to the wavelength of the optical field.

In this paper we propose a method to determine the 3D contour of large objects via a point-to-point subtraction of two phase-contrast images. We have called the result of this subtraction the phase-difference image, and it directly provides a modulo 2π phase map from which it is possible to recover the 3D contour. The experimental setup can be controlled in such a way that phase-unwrapping procedures (over a regularly modulo 2π phase map with high-contrast speckle noise) can usually be avoided. With this approach, only two interferometric registers are needed, reducing computation time and experimental complexity. Based on the description of our experimental setup, we theoretically model our method. Then numerical calculations on this model as well as experimental results are shown to prove the validity of this technique.

2. Phase-Difference Images

Let us consider the experimental setup illustrated in Fig. 1. A He–Ne laser beam is split by the variable beam splitter (VBS_1) into the object and reference beams, such that the correct reference–object beam (OB) ratio is attainable. An enlarged version [produced by beam expander (BE_1)] of the reference beam (RB) is directed by the M_1 and M_2 mirrors and by the BS_2 nonpolarized beam splitter (BS) into the CCD camera. The OB is sent toward the 50/50 BS_3 BS, which splits it into equal intensity parts and directs those toward the M_4 and M_5 mirrors. Initially, M_4 and M_5 mirrors are placed at the same distance from the center of the BS_3 BS and perpendicular to each other. By tilting the M_5 mirror at angle $\Delta\alpha'/2$ in the x''–z'' plane (where the $''$ stands for a coordinate system rotated with respect to the illustrated one), the beam reflected on it will be angularly displaced by an amount $\Delta\alpha'$ with respect to that coming from M_4. With the S_1 and S_2 shutters, the object illumination can be chosen from the two OBs, OB_1 and OB_2. These beams make an angle between them controlled by the tilt of the M_5 mirror. The chosen OB emerging from BS_3 is enlarged by BE_2 to illuminate the object. According to the setup of the M_4 and M_5 mirrors, different angles of the object's illuminations are achievable. BE_2 also modifies the effect of the tilt angle $\Delta\alpha'/2$ over the relative angular distance between OB_1 and OB_2. For analysis purposes, we will be calling the effective angular displacement between these beams $\Delta\alpha = \Delta\alpha'/M$ with M the magnification factor of BE_2. The optical field scattered from the object is mixed with the reference beam into BS_2 and then recorded by the CCD camera.

The intensity impinging on the CCD camera $I(x_h, y_h)$, called the hologram intensity, is proportional to the squared modulus of the superposition of the reference and object optical fields, and the (x_h, y_h) denotes coordinates in the hologram plane. Hence if we know the reference wave, by means of an inversion diffraction process of $I(x_h, y_h)$, the object optical field can be calculated.[11–13] In this experiment, the reference wave is a plane wave, and then when a similar wave illuminates the recorded intensity $I(x_h, y_h)$ this diffraction process can be recorded into a plane located at a distance z with coordinates (x_i, y_i). According to the holography theory,[23,24] that diffracted optical field will contain, among other terms, the complete information about the object optical field. In the Fresnel–Fraunhofer approximation, the reconstructed complex optical field $E(x_i, y_i, z)$ will be given by

$$E(x_i,\ y_i,\ z) = \frac{iE_0}{\lambda z}\exp\left[-\frac{i\pi}{\lambda z}\left(x_i^{\,2} + y_i^{\,2}\right)\right] \times \int_{-\infty}^{\infty}\int_{-\infty}^{\infty} I(x_h,\ y_h)\exp\left[-\frac{i\pi}{\lambda z}\left(x_h^{\,2} + y_h^{\,2}\right)\right] \times \exp\left[\frac{i2\pi}{\lambda z}\left(x_h x_i + y_h y_i\right)\right]\mathrm{d}x_h\mathrm{d}y_h, \qquad (1)$$

with z denoting the propagation distance, E_0 denoting the amplitude of the reconstruction field, and λ denoting the wavelength of the reconstruction field.

Since CCD cameras can acquire only a sampled version of $I(x_h, y_h)$ named $I(k, l)$, diverse numerical algorithms have been developed to obtain a discrete representation of the object optical field $[E(m, n, z)]$ at a distance z. All the algorithms are based on the calculation of the inverse diffraction process of $I(k, l)$ (Ref. 11); the discrete version of Eq. (1) is given by

$$E(m,\ n,\ z) = \frac{iE_0}{\lambda z}\exp\left[-\frac{i\pi}{\lambda z}\left(\frac{m^2}{N_x^{\,2}\Delta x_h^{\,2}} + \frac{n^2}{N_y^{\,2}\Delta y_h^{\,2}}\right)\right] \times \sum_{k=0}^{N_x-1}\sum_{l=0}^{N_y-1} I(k,\ l)\exp\left[-\frac{i\pi}{\lambda z}\left(k^2\Delta x_h^{\,2} + l^2\Delta y_h^{\,2}\right)\right]\exp\left[i2\pi\left(\frac{km}{N_x} + \frac{ln}{N_y}\right)\right]. \qquad (2)$$

Here a hologram intensity $I(k, l)$ spreads over an area of $N_x \times N_y$ pixels of the CCD sensor with $m = 0, 1, \ldots, N_x - 1$ and $n = 0, 1, \ldots, N_y - 1$. $\Delta x_h \times \Delta y_h$ denotes the CCD pixel size, and the image (reconstructed hologram) pixel size $\Delta x_i \times \Delta y_i$ is related to the CCD pixel size $\Delta x_h \times \Delta y_h$ by $\Delta x_i = \lambda z/(N_x \Delta x_h)$ and $\Delta y_i = \lambda z/(N_y \Delta y_h)$. This last expression determines the smallest detail that can be reconstructed; it has been regarded as the resolution of the digital holographic process.[11–13]

The calculated object field is expressed as a complex function of the discrete reconstruction coordinates (m, n) for a particular distance z. This allows us to numerically evaluate intensity, amplitude, and phase for this field. From Eq. (2), the intensity image of the object optical field can be calculated as

$$I(m, n, z) = E(m, n, z)E^*(m, n, z) = \mathrm{Re}^2[E(m, n, z)] + \mathrm{Im}^2[E(m, n, z)], \tag{3}$$

and the amplitude image is given by the square root of Eq. (3). Here "*" stands for the complex conjugate, and Re and Im denote the real and imaginary parts of the complex field $E(m, n, z)$, respectively. The phase-contrast image of the object optical field is given by

$$\phi(m, n) = \arctan 2\left\{\frac{\mathrm{Im}[E(m, n)]}{\mathrm{Re}[E(m, n)]}\right\}, \tag{4}$$

where the function arctan 2 accounts for the signs of the $\mathrm{Im}[E(m, n)]$ and $\mathrm{Re}[E(m, n)]$ in the computation of the inverse tangent function. The function $\phi(m, n)$ takes values from $-\pi$ to π, i.e., this phase-contrast image is a modulo 2π phase map. If the largest height of the object under study is comparable with the wavelength of the optical field, this phase image represents a height map of it, as is the case in digital holography microscopy.[20–22]

Several procedures can be found in the literature to produce a 3D contour of large objects by means of digital holography.[14–16,19] The most widely utilized techniques rely on the use of illumination with optical sources with multiple wavelengths or on the use of laterally displaced illumination to produce fringe projection systems. The calculation of the phase image that provides the information about the 3D contour of the object is obtained by means of phase-shifting techniques or by the evaluation of the phase of two holograms acquired with different wavelengths.

By taking into account the advantage provided by digital holography to directly obtain phase-contrast imagines, we can determine the 3D contour of large objects with the use of a single wavelength of illumination and only two holograms from the object under study. If we manage our experimental setup to illuminate the object with OB_1 (see text above for details), we can calculate a phase-contrast image $\phi_1(x, y) = 2\pi/\lambda[x \sin \alpha + h(x, y)\cos(\alpha)]$. Now if the object is illuminated by OB_2, the phase-contrast image will be $\phi_2(x, y) = 2\pi/\lambda[x \sin(\alpha + \Delta\alpha) + h(x, y)\cos(\alpha + \Delta\alpha)]$. Each image is randomly distributed between $-\pi$ and $+\pi$, since the roughness of the object is comparable with the optical wavelength. The phase-difference image $\Delta\phi(x, y) = \phi_2(x, y) - \phi_1(x, y)$ will be given by

$$\Delta\phi(x, y) = \frac{2\pi}{\lambda} 2 \sin\frac{\Delta\alpha}{2}\left[x \cos\left(\alpha + \frac{\Delta\alpha}{2}\right) - h(x, y)\sin\left(\alpha + \frac{\Delta\alpha}{2}\right)\right]. \tag{5}$$

The first term of this phase-difference image represents the linear phase provided by the carrier of the system, and it is totally independent of the object. This term is controlled by the relative angle between the OB_1 and OB_2 $\Delta\alpha$ and by the angle α that OB_1 makes with the $-z$ axis. The second term represents the phase introduced by the object. It must be unscrambled from the phase-difference image to get the object topography, i.e., the height map $h(x, y)$. According to Eq. (5), to recover $h(x, y)$, the phase introduced by the linear carrier should be subtracted from the phase difference, and thereafter the results should be inverted to obtain a positive version of the contour's object. The contour recovered by this procedure will be affected by a constant factor that entirely depends on the geometry of the setup.

When the phase-contrast images $\phi_1(x, y)$ and $\phi_2(x, y)$ are calculated from the recorded holograms, they are modulo 2π phase maps. Hence attention should be focused on the calculation of the phase-difference image $\Delta\phi(x, y) = \phi_2(x, y) - \phi_1(x, y)$, such that it will be given by

$$\Delta\phi(x, y) = \begin{cases} \phi_2(x, y) - \phi_1(x, y), & \text{if } \phi_2(x, y) \geq \phi_1(x, y), \\ \phi_2(x, y) - \phi_1(x, y) + 2\pi, & \text{if } \phi_2(x, y) < \phi_1(x, y), \end{cases} \tag{6}$$

$\Delta\phi(x, y)$ will also have modulo 2π phase. If this phase map contains 2π jumps, conventional phase-unwrapping algorithms can be used to remove the 2π ambiguities[10] to obtain the absolute phase-difference image and obtain the object's contour. It is worth mentioning that due to the random phase introduced in the phase-difference image by the roughness of the object, when the phase-unwrapping algorithms are needed, they will be a key point in the success of the 3D contouring of the object. However, as we will show in Section 3, our experimental setup can be adjusted to eliminate any 2π jumps in the phase-difference images, avoiding the need for phase-unwrapping algorithms.

3. Results and Analysis

In this section we show by means of numerical modeling and experimental results the validity of our proposal to determine the 3D contour of large objects.

Initially, we considered a sphere of 7.8 ± 0.1 mm in a radius illuminated by a red laser (632.8 nm). The

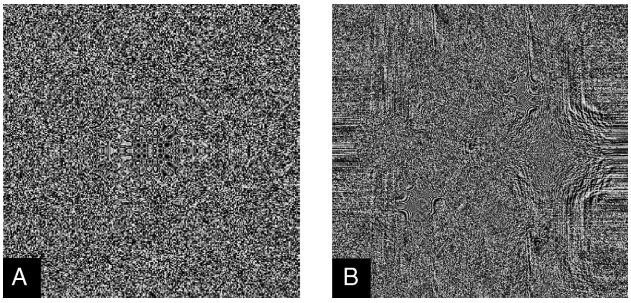

Fig. 2. Phase-contrast images directly obtained from the reconstructed holograms: A, numerical modeling; B, experimental result. In these images we have illuminated the object with OB_1. The phase-contrast images in both cases are random intensity distributions due to the surface roughness of the sphere. The results for OB_2 look alike.

illumination angle α was set to $23° \pm 1°$ with respect to the $-z$ axis, and the M_5 mirror was tilted $\Delta\alpha'/2 = 0.033° \pm 0.001°$ with respect to the M_4 mirror. The magnification of BE_2 was $|M| = 11$, then the effective angular displacement of OB_1 and OB_2 was set to $\Delta\alpha = 0.006° \pm 0.001°$. This feature of the system of producing smaller effective angular displacements than the actual tilt of M_5, allows us to avoid measurements of small angles and decreases an important source of error in this kind of application.

Phase-contrast maps for the experimental conditions stated above are shown in Fig. 2. Figure 2A shows a numerical model, and Fig. 2B shows experimental results. Only the images corresponding to OB_1 are shown, since the images for OB_2 look the same qualitatively. The phase distribution of the reconstructed object field for each OB illumination is randomly distributed between $-\pi$ and $+\pi$. These images do not provide direct information about the object under study, which is why the direct 3D contouring through phase-contrast images has only been applied to objects with dimensions comparable to the optical wavelength.[20,21] However, in the case of large objects, we can consider the difference between the phase-contrast images obtained with OB_1 and OB_2 as stated in Eq. (6). This phase-difference image will provide the 2π-modulo phase map about the object under study required in the 3D-contouring process.

The phase-difference image obtained from the point-to-point subtraction of the phase-contrast images when the object is illuminated with OB1 and OB2 is shown in Fig. 3. Figure 3A shows numerical modeling results, and Fig. 3C shows experimental results. These phase-difference images represent the modulo 2π phase map that, in other 3D-contouring approaches, is obtained by means of phase-shifting techniques[16] (Figs. 3A and 3C), or multiwavelength illumination[14,15] [Figs. 3B and 3D], for instance. To get the modulo 2π phase maps required in the 3D-contouring process, we do not require more than two images nor sophisticated and/or expensive multiwavelength systems, making this approach efficacious on many levels of research and education in optics.

If a direct phase-unwrapping approach is used over Figs. 3A–3C, an unwrapped map corresponding to a slanted sphere would be obtained. The slope of the plane associated with the distorted sphere is given by the linear carrier term presented in Eq. (5). To obtain an actual phase representation of the object under study, that term must be subtracted. Thanks to the fundamental feature of digital holography of providing full numerical manipulation of the phase and amplitude of the reconstructed optical field, the linear carrier term can be numerically subtracted from the phase-difference image. Figures 3B–3D show the phase-difference image after the linear carrier term has been subtracted for numerical modeling–experimental results. This new phase-difference image represents the actual phase introduced in the optical field by the object under study; in this case it shows the phase introduced by a sphere. Once more we state that these results are equivalent to those obtained with multiwavelength contouring systems, but in our case we require only a unique wavelength.

After subtracting the linear carrier term and inverting the result, a direct 3D representation of the phase-difference image will lead us to a model of the object under study within a reference frame in phase units. To get the 3D representation of the object in metric units, we just multiply that phase-difference image times the geometric factor given by the experimental setup. Figure 4A shows the numerical model results, and Fig. 4B shows the experimental results.

The 3D shape is successfully reconstructed in the numerical modeling as well as in the experimental results. The measured dimensions in both cases are in good agreement with the measurements made with a micrometer. In the numerical modeling, we report a radius of 7.8 ± 0.1 mm, whereas in the experiment, a radius of 7.5 ± 0.3 mm is registered. Despite having both measurements being close to the measurement by the other method, the relationship

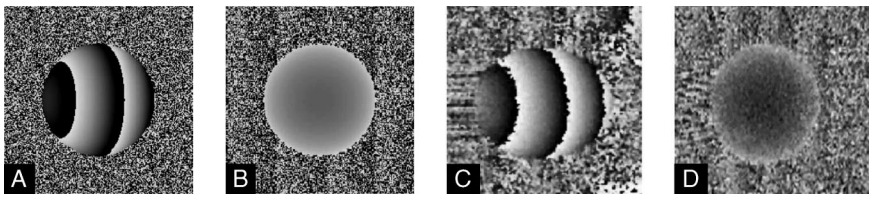

Fig. 3. Phase-difference image numerical modeling results of subtracting the phase-contrast maps obtained by illuminating with OB_1 and OB_2: A, before and B, after subtraction of the linear carrier term in Eq. (5). C and D show the same information for the experimental results.

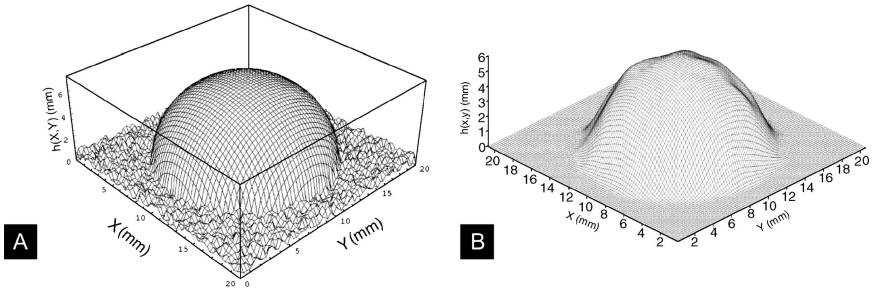

Fig. 4. Three-dimensional reconstruction via phase-difference images: The original object, a semisphere 7.80 ± 0.05 mm in radius, is successfully reconstructed using A. numerical modeling and B. experimental setup.

between the accuracy of our method and the sensitivity of the optical systems must be studied. To carry out this study, we chose as an object, a pyramid, for which we have measured a height of 11.50 ± 0.05 mm with the micrometer. We have chosen this object for this study because its slanted surfaces and its abrupt change of slope are challenging for any noncontact topographic technique.

The height-change $\Delta h(x, y)$ in the object that produces a 2π change in the phase-difference image is given by

$$\Delta h(x, y) = \frac{\lambda}{2 \sin \frac{\Delta\alpha}{2} \sin\left(\alpha + \frac{\Delta\alpha}{2}\right)}, \tag{7}$$

and it can be recognized as the sensitivity of the system.[16] It is fully determined by the wavelength and the geometry of the experimental setup such that for a fixed illumination angle α, by simply changing the tilt angle of the M_5 mirror, we can achieve different values of sensitivity. This feature makes it possible to set up the tilt angle such that the number of 2π jumps in the phase-difference image can be controlled for any type of object under study. In our former example, we utilized this feature to set up the sensitivity such that no 2π jumps were present in the phase-difference image, avoiding the unwrapping process.

In Fig. 5 we show the phase-difference image before (Fig. 5A) and after (Fig. 5B) subtracting the linear carrier in an experiment with the pyramid model. Illumination angle α was set to 23° ± 1° and the effective angular displacement of OB_1 and OB_2 was $\Delta\alpha = 0.006° \pm 0.001°$. This configuration leads us to a sensitivity of 15.45 mm, and the measured height of the pyramid was 11.5 ± 0.3 mm. The rapid change of slope at the base of the pyramid introduces a high-frequency noise in this region (see Fig. 5B), which

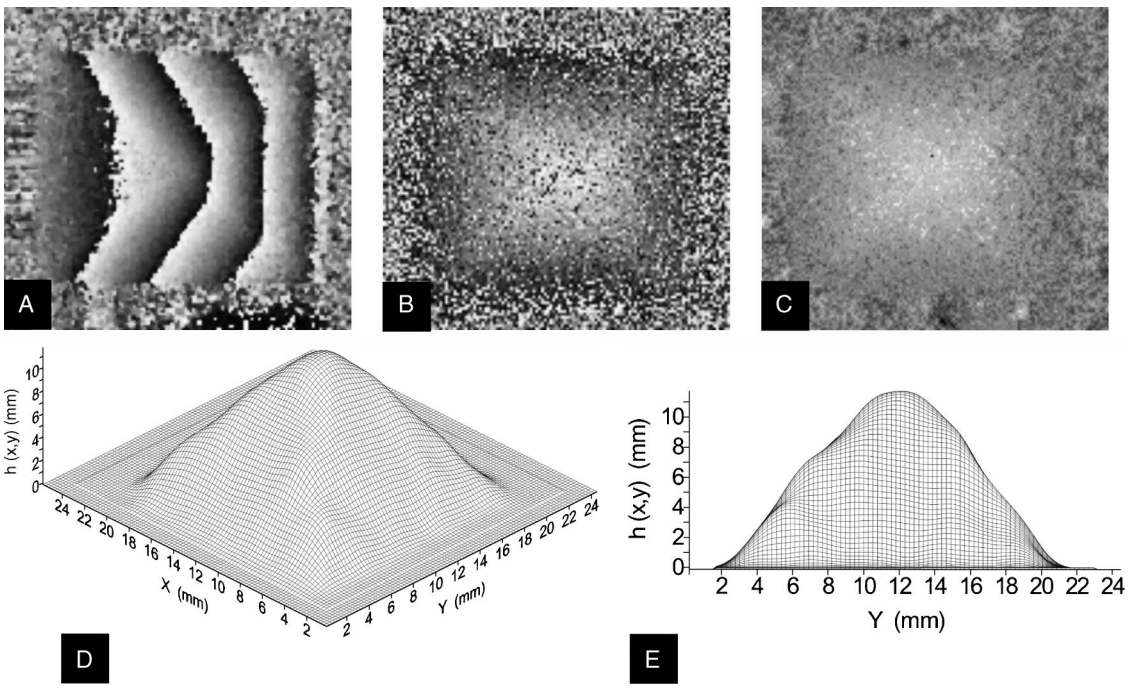

Fig. 5. Experimental 3D reconstruction via phase-difference images. The original object, a pyramid 11.50 ± 0.05 mm in height, is successfully reconstructed. The phase-difference images, A, before and B, after the subtraction of the linear carrier, show the need for using phase-unwrapping techniques. The resulting unwrapped phase difference C leads us to the D, 3D representation and E, the side view.

Table 1. Experimental Study of the Effect of the Sensitivity on the Method of 3D Reconstruction by Phase-Difference Images[a]

$\Delta\alpha$ (deg 10^{-4})	Δh (mm)	Measured h (mm)	Phase-Difference Image: Before Subtraction of Linear Carrier	Phase-Difference Image: After Subtraction of Linear Carrier	Side View of the Pyramid's 3D Reconstruction
30	30.9	11.5	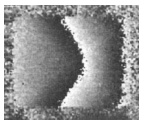	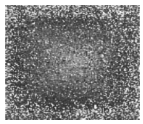	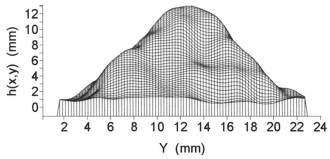
46	20.6	11.5	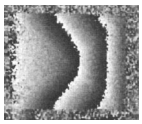	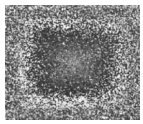	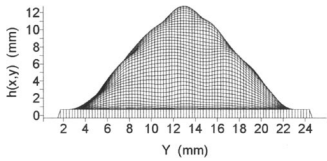
60	15.45	11.5	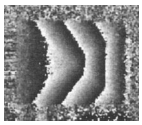	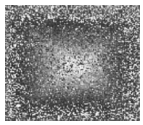	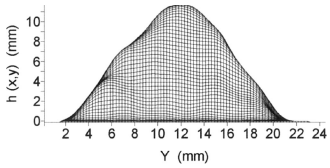
90	10.3	10.5	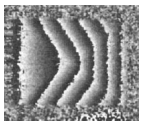	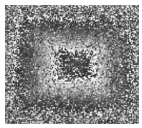	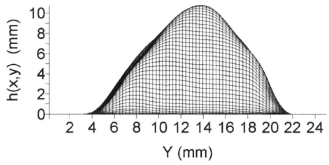
120	7.73	10.5	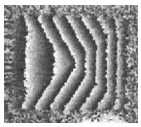	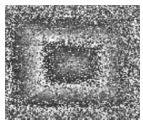	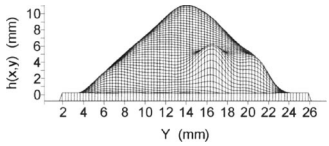
136	6.87	10.5	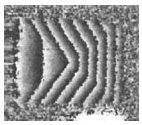	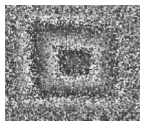	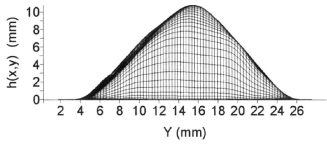
150	6.18	9.5	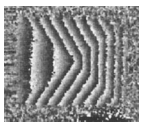	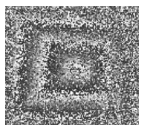	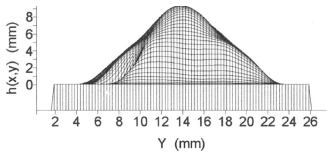

[a]Phase-difference image with 2π jumps after subtraction introduces deviation on the measured height from the real value. Those 2π jumps can be avoided by the proper setting of the optical setup; see text for details.

makes it necessary to use phase-unwrapping techniques.[10] The resulting unwrapped phase-difference image is shown in Figs. 5C and 5D with its 3D representation after the multiplication by the geometric factor; a side view of the object for easy measurement, of the pyramid height has been shown in Fig. 5E.

Table 1 shows the phase-difference images before and after the subtraction of the linear carrier for different experiments with our pyramid. The illumination angle α was set to $23° \pm 1°$, and the effective angular displacement of OB_1 and OB_2 was varied from $\Delta\alpha = 0.003° \pm 0.001°$ to $\Delta\alpha = 0.015° \pm 0.001°$, leading us to sensitivity values ranging from 30.9 ± 0.1 mm to 6.18 ± 0.1 mm. A side view of the 3D reconstruction is also shown for height measurement purposes. The measured height of the pyramid is in good agreement with its real value of 11.50 ± 0.05, and the sensitivity is greater than this value. The reason for this behavior is that, after this limit, 2π jumps will be present in the phase-difference image, and the phase-unwrapping process will distort the performance of the method. Fortunately the sensitivity of this system can be easily adjusted such that no 2π jumps are present in the phase-difference image after subtraction of the linear carrier, avoiding the use of phase-unwrapping procedures. This feature led us to successful results such as those shown in Figs. 4 and 5.

4. Conclusion

Digital holography allows for the numerical reconstruction of the object wavefront from a digitally recorded hologram. This computational approach to holography permits calculating amplitude- and phase-contrast images from objects under study. The phase-contrast images can be used directly to obtain the 3D contour of microscopic objects but not large ones.

By subtracting point-to-point phase-contrast images of large objects, we have shown the feasibility of obtaining 3D contours of large objects. These phase-contrast images are acquired by different angle illuminations of the object. Numerical modeling and experimental results have led to the conclusion of the efficiency of the method.

The effect of the sensitivity of the experimental setup on the 3D-contouring method has been analyzed. We conclude that the presence of 2π jumps ruins the efficiency of our method due to the need for phase-unwrapping processes. Fortunately, the proposed experimental system can be set to the right conditions such that no 2π jumps are present, and the phase-unwrapping stage can be skipped, avoiding the many times bottleneck in optical metrology studies.

The authors thank DIME (División de Investigaciones Sede Medellin) and Universidad EAFIT (Dirección de Investigación y Docencia, proyecto número PY0313) for support during the period of this research. They also thank Peter Klages and Kris Barstow for their inspiring reading of this manuscript.

References

1. D. C. Williams, *Optical Methods in Engineering Metrology* (Chapman & Hall, 1993).
2. L. Chen and C. Quan, "Fringe projection profilometry with nonparallel illumination: a least-squares approach," Opt. Lett. **30,** 2101–2103 (2005).
3. H. Cline, W. Lorensen, and A. Holik, "Automatic moire contouring," Appl. Opt. **23,** 1454–1459 (1984).
4. O. Kafri and I. Glatt, *The Physics of Moire Metrology* (Wiley, 1990).
5. B. Hildebrand and K. Haines, "Multiple-wavelength and multiple-source holography applied to contour generation," J. Opt. Soc. Am **57,** 155–162 (1967).
6. J. Zelenka and J. Varner, "Multiple-index holographic contouring," Appl. Opt. **8,** 1431–1434 (1969).
7. P. DeMattia and V. Fossati-Bellani, "Holographic contouring by displacing the object and the illumination beam," Opt. Commun. **26,** 17–21 (1978).
8. R. Jones and C. Wykes, *Holographic and Speckle Interferometry* (Cambridge U. Press, 1983).
9. K. Creath and J. Wyant, "Absolute measurement of surface roughness," Appl. Opt. **29,** 3823–3827 (1990).
10. D. Malacara, M. Servín, and Z. Malacara, *Interferogram Analysis for Optical Testing* (Marcel Dekker, 1998).
11. L. P. Yaroslavskii and N. S. Merzlyakov, *Methods of Digital Holography* (Consultants Bureau, 1989), translated from Russian by D. Parsons.
12. U. Schnars and W. P. O. Juptner, "Digital recording and numerical reconstruction of holograms," Meas. Sci. Technol. **13,** R85–R101 (2002) and the reference therein.
13. U. Schnars and W. P. Jueptner, *Digital Holography* (Springer-Verlag, 2005).
14. Y. Zou, G. Pedrini, and H. J. Tiziani, "Surface contouring in a video frame by changing the wavelength of a diode laser," Opt. Eng. **35,** 1074–1079 (1996).
15. C. Wagner, W. Osten, and S. Seebacher, "Direct shape measurement by digital wavefront reconstruction and multiwavelength contouring," Opt. Eng. **39,** 79–85 (2000).
16. I. Yamaguchi, S. Ohta, and J. Kato, "Surface contouring by phase-shifting digital holography," Opt. Lasers Eng. **36,** 417–428 (2001).
17. T. Zhang and I. Yamaguchi, "Three-dimensional microscopy with phase-shifting digital holography," Opt. Lett. **23,** 1221–1223 (1998).
18. G. Pedrini, P. Froning, H. J. Tiziani, and F. Mendoza Santoyo, "Shape measurement of microscopic structures using digital holograms," Opt. Commun. **164,** 257–268 (1999).
19. L. Z. Cai, Q. Liu, X. L. Yang, and Y. R. Wang, "Sensitivity adjustable contouring by digital holography and a virtual reference wavefront," Opt. Commun. **221,** 49–54 (2003).
20. E. Cuche, F. Bevilacqua, and C. Depeursinge, "Digital holography for quantitative phase-contrast imaging," Opt. Lett. **24,** 291–293 (1999).
21. J. Gass, A. Dakoff, and M. K. Kim, "Phase imaging without 2π ambiguity by multiwavelength digital holography," Opt. Lett. **28,** 1141–1143 (2003).
22. M. Sebesta and M. Gustafsson, "Object characterization with refractometric digital Fourier holography," Opt. Lett. **30,** 471–473 (2005).
23. R. Colier, C. Burckhardt, and L. Lin, *Optical Holography* (Academic, 1971).
24. J. W. Goodman, *Introduction to Fourier Optics* (McGraw-Hill, 1968).